INSTITUTE OF PHYSICS PUBLISHING JOURNAL OF MICROMECHANICS AND MICROENGINEERING

J. Micromech. Microeng. **14** (2004) 632–638 PII: S0960-1317(04)70175-8

A polymeric piezoelectric micropump based on lamination technology

Thai-Quang Truong and Nam-Trung Nguyen

School of Mechanical and Production Engineering, Nanyang Technological University, 50 Nanyang Avenue, 639798 Singapore

E-mail: quangtt@pmail.ntu.edu.sg

Received 9 October 2003, in final form 14 January 2004
Published 6 February 2004
Online at stacks.iop.org/JMM/14/632 (DOI: 10.1088/0960-1317/14/4/026)

Abstract

This paper presents the first micropumps assembled using polymeric lamination technology. Each pump consists of two 100 μm thick, 10 mm diameter SU-8 discs; two 1.5 mm thick, 15 mm diameter polymethylmethacrylate (PMMA) discs; and one piezo disc. The SU-8 parts were fabricated by a two-mask polymeric surface micromachining process with silicon as the sacrificial material. Each SU-8 disc has one micro check valve. The valve is a 1 mm plate suspended on a compliant orthoplanar spring. The cross section of the spring beam has a dimension of 100 μm $\times$ 100 μm. The PMMA parts were machined from an extrusion PMMA sheet by CO_2 laser. An off-the-shelf piezo bimorph disc worked as both actuator and pump membrane. The pump was assembled using adhesive bonding. The adhesive tapes were cut by the same laser system. Alignment pins were used in the assembly process. With a drive voltage of $\pm$150 V the fabricated micropumps have been able to provide flow rates up to 2.9 ml min^{-1} and back pressures up to 1.6 m of water. The pump design and the polymeric technologies prove the feasibility of making more complex microfluidic systems based on the presented lamination approach.

1. Introduction

In recent years, lab on a chip (LOC) has been attracting the interest of both industry and research community. Commercial LOCs are often made of polymers to achieve low cost, good biocompatibility and good chemical resistance [1]. The transport of fluid in LOCs can be provided by micropumps. However, most of the existing micropumps are fabricated by silicon micromachining, which involves relatively high temperatures [2–8]. The high temperature condition makes the integration of silicon micropumps incompatible with the polymeric processes.

One solution for the problem is making the entire LOC in silicon. Several such devices have been fabricated [9]. The drawbacks of this solution are complex fabrication processes and possible incompatibility with bio-samples. Furthermore, LOCs often have large sizes to accommodate the required long channels. The need for a large silicon area makes such devices even more expensive.

Another promising trend is to design polymeric micropumps which can be easily implemented in the polymeric fabrication process of LOCs. Polymeric micropumps, fabricated by microinjection moulding [10], hot embossing [11] and conventional machining [12] have been reported. The polymeric fabrication techniques mentioned are suitable for low-cost and mass production [9]. However, they are not ideal for prototyping, small and medium scale production due to high cost and long process time to fabricate the moulds. In [13], we reported a micropump fabricated with a layered concept. The pump consisted of SU-8 check valves fabricated by polymeric surface micromachining techniques, and polymethylmethacrylate (PMMA) plates machined by milling tools. Four bolts were used to fix the structure. The pump served well to demonstrate the feasibility of the layered concept. However, it had several shortcomings: lack of alignment features, high leakage and high spring stiffness. The four bolts also made the pump very bulky.

This paper presents an improved version of the pump reported in [13]. New valve designs and fabrication technologies have been implemented. First, three new valves with sealing rings have been designed in order to reduce leakage and to lower spring constants. The fabrication

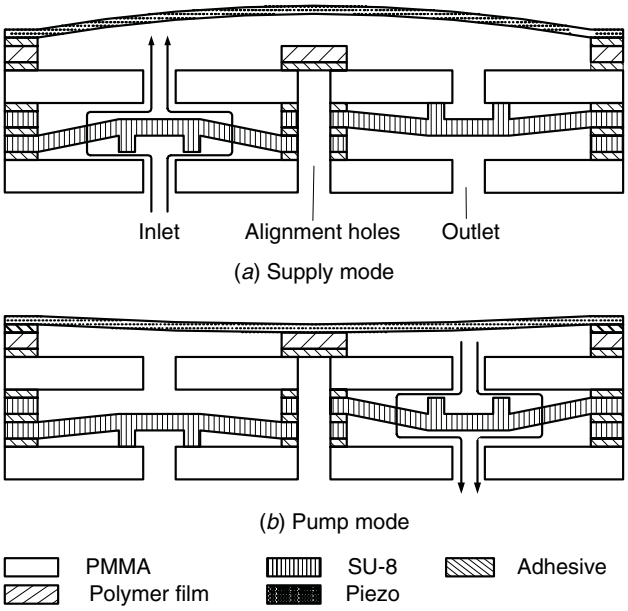

Figure 1. Schematic of the pump structure and is operation (not to scale). (*a*) Supply mode; (*b*) Pump mode.

of the SU-8 valves involved a two-mask polymeric surface micromachining process with silicon directly used as the sacrificial material. Second, laser micromachining was used in combination with polymeric surface micromachining. Relatively large parts were fabricated by laser machining, while size-critical parts were made with standard photolithography processes. Third, low-temperature adhesive bonding was used for laminating different polymer layers. The lamination technique is flexible and can be extended to more complex microfluidic systems. This paper also presents the improved performance of the fabricated micropumps.

2. Micropump design

2.1. The pump structure

The pump consists of five structural layers: the piezo bimorph disc, the top PMMA plate, two SU-8 discs and the bottom PMMA plate. These layers are bonded by four adhesive layers, figure 1.

The piezo bimorph disc is a brass plate 15 mm in diameter and 100 μm thick. A 90 μm thick layer of piezo ceramic is glued on top of the brass plate. The piezo bimorph disc works as both the actuator and the pump membrane.

The top and bottom PMMA plates are identical. Each plate measures 15 mm in diameter and 1.5 mm thick. It has two through-holes for fluid access, and two other alignment holes. The fluid accesses are 0.6 mm in diameter. The alignment holes have a diameter of 1.6 mm. The space between the top PMMA plate and the piezo disc defines the pump chamber. Two fluid accesses of the bottom PMMA plate are fitted with two metal needles used as inlet and outlet.

The two SU-8 discs are identical too. Both are 10 mm in diameter and 100 μm thick. The top SU-8 disc contains the outlet valve while the inlet valve is implemented in the bottom disc. The design and fabrication of the SU-8 disc are discussed later in sections 2.2 and 3.1.

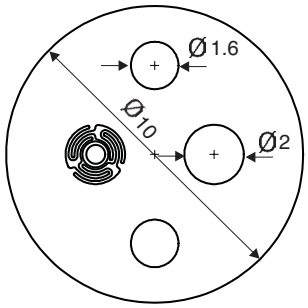

Figure 2. The geometry of the SU-8 disc (dimensions are in mm).

For alignment purposes, two alignment holes are incorporated in each of the PMMA plates and SU-8 discs. Assembly of the pump is achieved with two alignment pins and the corresponding alignment holes. These alignment holes are later covered by a polymer film. Figure 1 illustrates the pump structure and its operation.

2.2. Design of the SU-8 check valves

The basic design of a SU-8 disc is depicted in figure 2. The disc has one check valve, one inlet hole and two alignment holes. The check valve consists of a 1 mm valve disc suspended on N folded beams, which have a cross section of 100 μm $\times$ 100 μm. The beams work as valve springs connected in parallel [1]. The valve disc has a sealing ring, which is 100 μm thick. Its outer diameter and inner diameter are 0.9 mm and 0.6 mm, respectively. The ring offsets the 50 μm gap, which was created by the adhesive layer, between the valve disc and the fluid access holes. The ring also creates a pre-loaded condition for the springs to reduce leakage. The micropump previously reported in [13] used SU-8 valves with four folded beams as springs [13]. The four folded beams resulted in a relatively high spring constant. Thus, a high pressure was needed for opening the valve. In order to lower the spring constant, we could reduce the number of beams. Valve designs with one or two folded beams could have spring constants 20 times lower than that of the four beams [1]. However, the valve discs of these designs may suffer rotation movement and cause high leakage rates. Two new valve designs with three folded beams are presented in this paper. These designs have lower spring constants, and at the same time secure the out-of-plane motion of the valve disc. Figure 3 depicts the three valves implemented in the micropumps reported in this paper. The details of the designs and geometrical parameters are shown in figure 3.

Numerical simulation with ANSYS was used to find the spring constants of the valves. A pressure of 3000 Pa was applied to the valve disc. The Young's modulus of SU-8 was assumed to be 4.02×10^9 Pa. The spring constant was determined by the force and the simulated displacement (1):

$$k = \frac{F}{\delta} = \frac{p\pi r^2}{\delta}, \tag{1}$$

where k is the spring constant, F is the force applied on the valve disc, p is the pressure, r is the radius of the valve disc and δ is the displacement. The results in figure 3 show that valve 3 (*c*) is three and two times softer than valve 1 and valve 2, respectively.

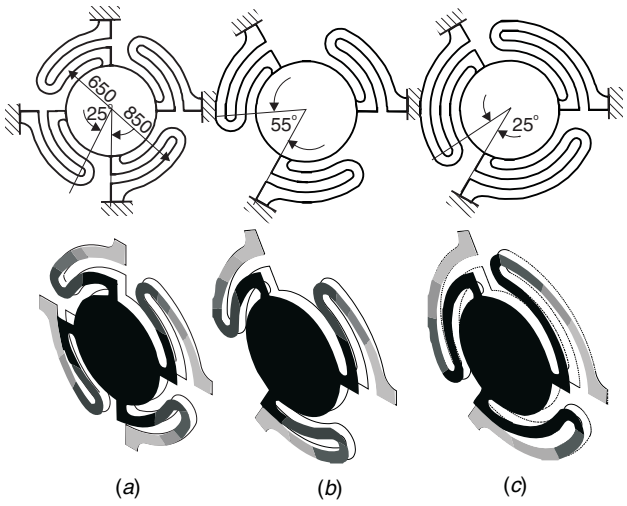

Figure 3. Three different valve designs result in three different spring constants (dimensions are in microns). Results obtained by FEM. (*a*) Valve 1, 4 springs, $k = 927$ N m^{-1}; (*b*) valve 1, 3 springs, $k = 691$ N m^{-1}; (*c*) valve 3, 3 extended springs, $k = 286$ N m^{-1}.

The rectification behaviour of the valves was simulated using the semi-analytical coupled fluid-structural technique [1]. As discussed, the valve designs in this paper ensure the parallel displacement of their valve discs. Therefore, each valve can be modelled as a disc connecting to a spring. The spring constant of each valve was determined in the previous paragraph. This spring constant can then be used for a semi-analytical coupled simulation described next. The coupling was realized in an iteration loop written as a macro script in the ANSYS batch file. First, the flow analysis was carried out for an initial gap between the valve disc and the inlet. The pressure distribution across the valve disc was used with the known stiffness for calculating the displacement analytically. The new gap between the valve disc and the inlet was then updated. The flow model was then meshed again with the new geometry, readied for the following iteration. The iteration loop stopped if the displacement difference reached a given convergence condition which was 10 nm in our analysis. On average, the coupled simulation stopped after three or four iterations.

The rectification behaviour is defined by the flow rate–pressure characteristics in both flow directions. Typical results in reverse and forward directions are depicted in figures 4(*a*) and (*b*), respectively. The left side of figure 4 shows the pressure distribution, while the right side shows the velocity field in the valves. The rectification characteristics are compared with the measurement results later in section 4.1.

3. Fabrication

3.1. SU-8 disc

The SU-8 discs were fabricated using the basic polymeric surface micromachining techniques, which were described in detail in [1]. However, further developments of this process were implemented in the fabrication of the three new valve designs. First, a two-mask process was used for fabricating microvalves with sealing ring. Second, the basic process in [1] was simplified by using silicon directly as the sacrificial material.

The process started with spin-coating SU-8 2100 photoresist (Microchem Corp., USA) on silicon, figure 5(*a*). This first SU-8 was then soft baked and exposed to UV light using the first mask containing all features of the SU-8 disc except the ring, figure 5(*b*). The intended thickness of this SU-8 film was 100 μm.

After hard baking, a second 100 μm thick SU-8 layer was spin-coated on top of the first layer. After a soft-baking step, the second mask containing the ring design was used for the second exposure, figure 5(*c*). The second mask was aligned to the first SU-8 layer using alignment marks. Even though

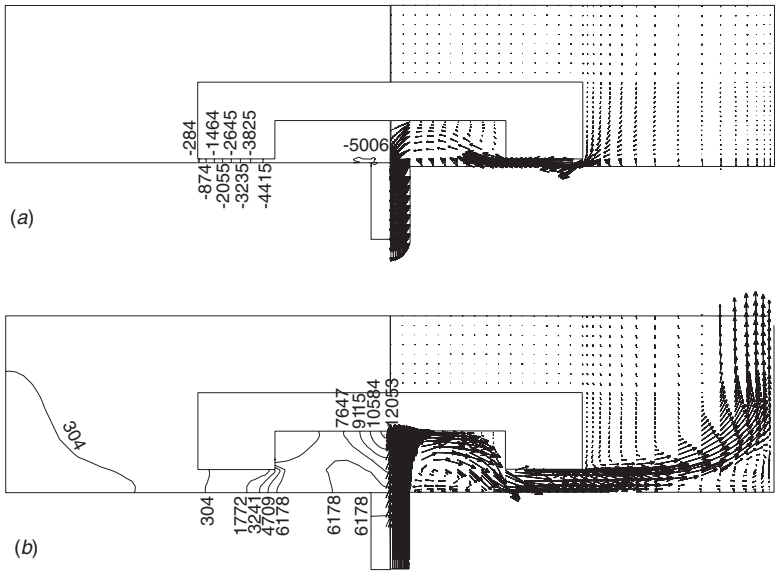

Figure 4. Coupled fluid-structural simulation, the left and right sides show the pressure distribution and the velocity field, respectively: (*a*) reverse flow; (*b*) forward flow.

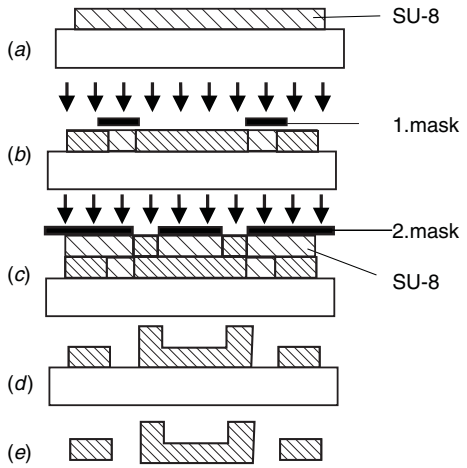

Figure 5. Process steps for the SU-8 valve disc.

the first SU-8 layer had not been developed, the alignment marks were still visible. The visible alignment marks were made possible by the different optical indices between cross-linked SU-8 and the unexposed area. With this two-mask process we achieved an accuracy of 10 μm, which satisfied our application.

After the second UV exposure, the two SU-8 layers were hard baked and cooled down to room temperature. They were then developed using propylene glycol methyl ether (PGMEA), figure 5(*d*).

In the final steps, the SU-8 discs were released in 30% KOH solution. Etch access created by many circular holes on the discs allows fast under etching. The circular shapes and the smooth designs circumvent the anisotropic characteristics of the KOH etch process. After releasing the SU-8 discs were cleaned with deionized (DI) water and dried with nitrogen.

Figure 6 shows the SEM (scanning electron microscopy) images of valve 2 and valve 3. For this purpose, a thin aluminium layer was sputtered on the SU-8 surface. The holes on the discs have two functions: allowing fast release and arresting residual stress on the discs. Stress may cause micro cracks in the SU-8 structures. Cracks are a serious problem for SU-8 structures, especially for a moveable structure such as our folded beams. In addition to the holes and smooth designs, the temperature recipes in our process were also optimized. As a result no cracks can be detected in these SU-8 structures. Furthermore, good alignment of the second mask can be seen with the ring precisely placed on top of the valve plate.

3.2. PMMA and adhesive parts

The PMMA plates were cut out from a 1.5 mm thick PMMA sheet (extrusion type). They were designed in Autocad and sent to a laser cutter (Universal Laser Systems, M-300, 25 W). The system can deliver a maximum laser power of 25 W and a maximum scanning velocity of 640 mm s^{-1} at a resolution of 1000 dpi. The power and the cutting speed for the PMMA parts were set at 9% and 1.1% of the maximum values, respectively.

The adhesive parts were cut out from a transfer adhesive tape (Adhesives Research, Inc, Arclad 8102 transfer adhesive). The transfer adhesive tape consists of a carrier and a 50 μm thick adhesive layer. The laser power and the cutting speed for the adhesive tape were set at 1% and 1.1% of the maximum values, respectively.

The polymer layer covering the alignment holes was cut out from a 100 μm thick overhead projector transparency sheet (3M, PP2500) covered by the transfer adhesive tape. The laser power and cutting speed for these layers were set at 3% and 1.1% of the maximum values.

3.3. Assembly procedure

Figure 7 shows the assembly sequences of the micropump. First, the bottom PMMA plate was slotted into the alignment pins, followed by the first adhesive disc with the carrier facing

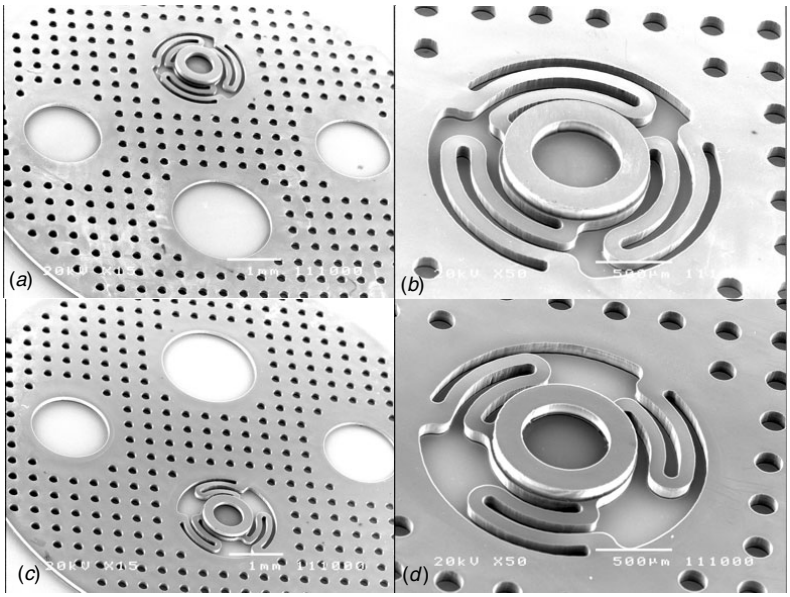

Figure 6. SEM picture of SU-8 check valves. (*a*) Top view, whole SU-8 disc, valve 2; (*b*) close-up of valve 2; (*c*) top view, whole SU-8 disc, valve 3; (*d*) close-up of valve 3.

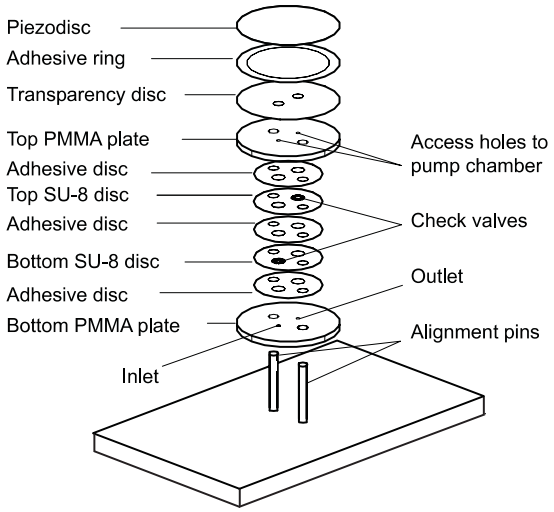

Figure 7. Lamination assembly concept of the micropump.

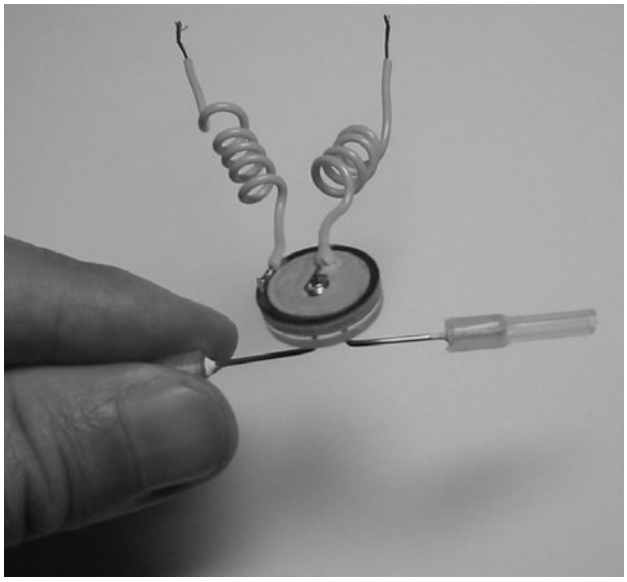

Figure 8. The assembled micropump.

up. The two layers were then pressed to bond. The carrier was then removed using two needles.

Next, the bottom SU-8 disc with the sealing ring facing down was placed on the stack. Subsequently, the second adhesive disc was laminated on top of the SU-8 disc; its carrier was then removed. In the following step, the top SU-8 disc with its ring facing up was assembled. The third adhesive disc was later laminated in the same manner as for the first two.

The top PMMA plate was then placed on top of the stack. The whole stack was pressed to achieve good bonding. The inlet and outlet were marked. The bonded stack was then removed from the alignment pins. The carrier of the polymeric disc was removed.

In the following step, the polymer layer covering the alignment holes was aligned to and pressed against the top PMMA plate. Next, the adhesive ring with the adhesive layer facing down was placed on top of the polymer disc. The carrier of the ring was removed, ready to bond with the piezo disc. The piezo disc was aligned and pressed on the pump stack. Finally, two syringe needles, 0.65 mm in diameter, were attached to the inlet and outlet by epoxy glue (Araldite, Super rapid epoxy). The assembled pump, measuring 15 mm in diameter and 3.8 mm thick, is shown in figure 8.

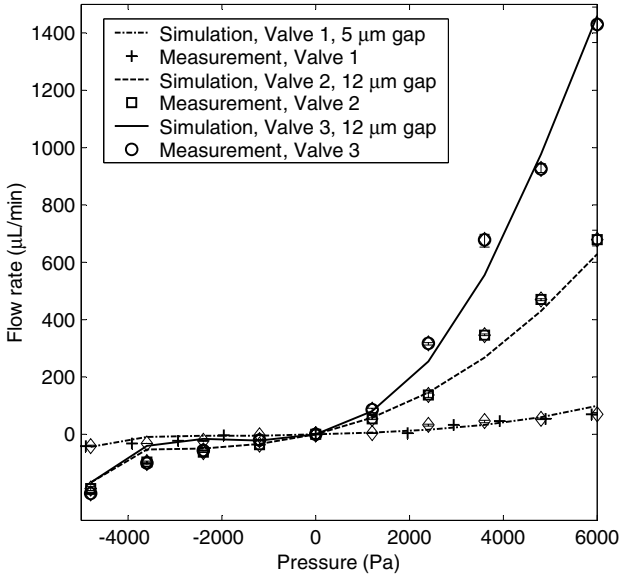

Figure 9. Measured and simulated behaviour of valve 1, valve 2 and valve 3.

4. Experimental results

4.1. Micro check valves

The three valve designs shown in figure 3 were first characterized as stand-alone devices. The flow rectification behaviours of the valves were tested with deionized water following the procedure in [1]. The flow characteristics of the valves were taken by measuring the pressure drop across the valve and the corresponding volumetric flow rate. The volumetric flow rate is determined by the travel speed of the water/air interface in a capillary with a known diameter. A large reservoir with different heights of the water surface emulates the inlet pressure and eliminates the error of height change during the measurement. The pressure drop was measured with a differential pressure sensor (Honeywell 22PC-Series, ± 1 psi) which was calibrated for a pressure range 0–6000 Pa. The outlet of the valve was connected to a horizontal capillary with an inner diameter of 0.8 mm. The travel speed of the meniscus was determined by measuring the travel time over a fixed distance and converted into the flow rate.

Each valve was measured several times. The average flow rates are plotted in figure 9. The maximum and minimum flow rates at each frequency of each valve are plotted as error bars. The measurement error is approximately 5%.

The coupled fluid-structural simulation results were fitted to the measurements by adjusting the initial gap between the valve disc and the inlet/outlet. The initial gaps of valve 1, valve 2 and valve 3 were set at 5 μm, 12 μm and 12 μm, respectively. The simulation results agree well with the measurements, see figure 9. This good agreement proves the

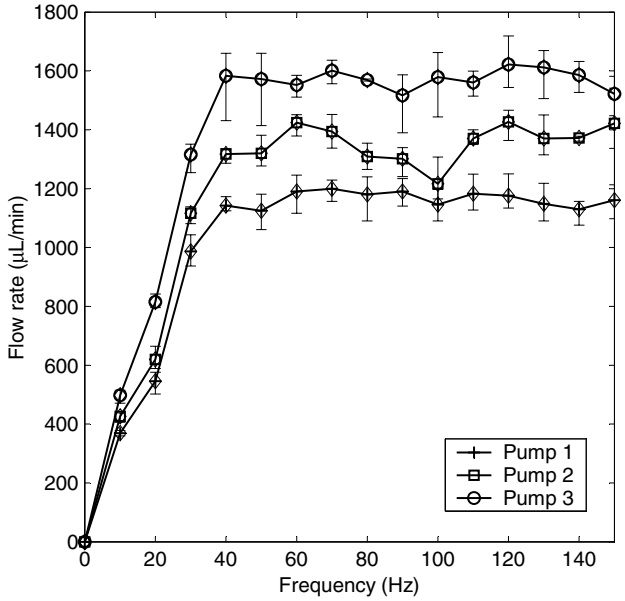

Figure 10. Flow rate versus frequency ($V = 100 \pm$ V). Measurement data.

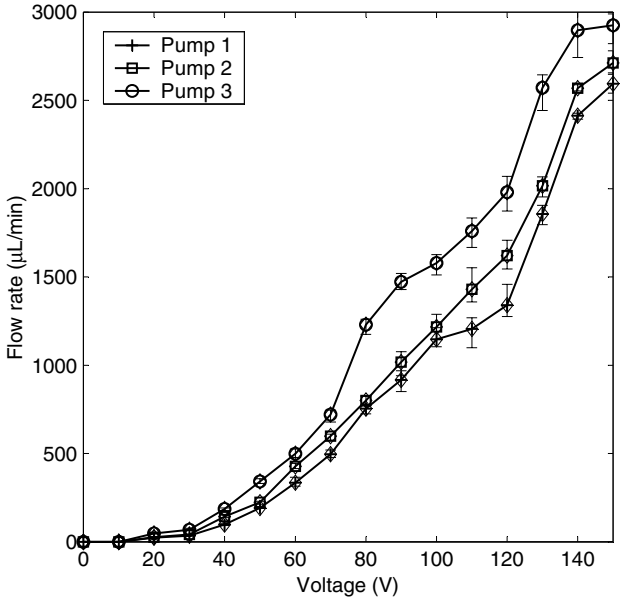

Figure 11. Flow rate versus voltage (frequency = 100 Hz). Measurement data.

validity of the coupled fluid-structural simulation technique, provided that appropriate initial gaps are set. The effect of initial gaps on the behaviour of the valve stresses the importance of a good sealing.

Valve 1 does not have a clear rectification behaviour, while valves 2 and 3 do, see figure 9. Valve 1 has a low flow rate in the forward region, due to its high spring constant. The leakage rates in the reverse region of all three valves are small compared to those of the valves reported in [1]. The reason for the improvement is the better sealing, created by the springs, which is pre-loaded by 50 μm.

4.2. Micropumps

Three pumps were assembled by the lamination technique described in 3.3. Each micropump was equipped with a micro check valve discussed above. The pumps were characterized using a simple setup described in a previous paper [15]. The working fluid was DI water. The pumps needed to be primed using a syringe before testing. The pumps were characterized similar to the valves. Each pump was also measured several times to obtain the average measurements. Maximum measurements and minimum measurements represent error bars. The measurement errors for pumps characterizations are also around 5%.

Figure 10 shows the measured flow rates versus the actuating frequencies at the voltage of ±100 V (peak–peak). The measured flow rates versus actuating voltages characteristics at the frequency of 100 Hz are shown in figure 11. Finally, figure 12 shows the flow rates versus back pressures at ±100 V and 100 Hz. The three pumps show significant improvement over the pump reported in [13]. It is evident that the pump's performances are closely related to the spring constants of the valves. Pump 3 has the best performance due to its lowest spring constant. Pump 3 achieved a flow rate upto 2.9 ml min^{-1} and back pressures up to 160 cm of water (under a voltage of ±150 V), that

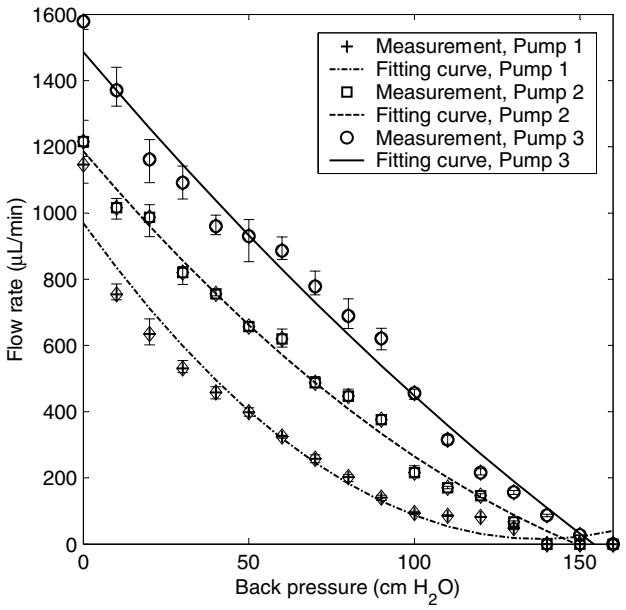

Figure 12. Flow rate versus back pressure ($V = 100 \pm$ V, frequency = 100 Hz).

is nearly three times the flow rate (1 ml min^{-1}) and eight times the back pressure (0.2 m) of the pump in [13]. Pump 3 delivers almost 24 times of the pumping power compared to the previous pump. The pumping power is estimated by (2):

$$P_{\text{pump}} = \frac{Q_{\max} \times p_{\max}}{2} \tag{2}$$

where P_{pump} is the pumping power, $p_{\max}$ and $Q_{\max}$ are the maximum back pressure and the maximum flow rate, respectively.

The reasons for the improvements are:

- better alignment between the two valves and of the valves to the inlet and outlet;

- better seal between the valve disc and the inlet/outlet thanks to the pre-loaded spring;
- lower spring constant valve design.

Compared to the previously reported pump [13], the pumps presented in this paper improved not only the performance but also are smaller, easier to assemble and easier to integrate. The pumps measure 15 mm in diameter and 3.8 mm thick, while the previous pump measures 30 mm × 30 mm × 4.5 mm. Due to the lamination assembly technique and the layered concept, these pump designs can be readily integrated into any polymeric microfluidic system.

Figure 12 shows nonlinear behaviours of the flow rate versus back pressure curves. While most mechanical pumps in the literature have linear flow rate versus back pressure behaviour [2, 3], micropump with nonlinear behaviour was also reported [16]. We think that the nonlinearity of the flow rate versus back pressure may be the consequence of dependence between the pressure produced by the pump and the back pressure.

The pumps discussed here are not self-priming. The reason is their relatively large dead volumes, which are the results of the inlet holes and outlet holes of the 1.5 mm thick PMMA plates. We are experimenting with thinner PMMA plates in order to reduce dead volume and achieve self-priming.

5. Conclusion

We have designed, fabricated and characterized the first fully polymeric piezo-actuated micropumps assembled by lamination technique. The main advantages of the pumps are modular design, low cost, simple fabrication and assembly processes. All fabrication and assembly processes, except for SU-8 parts, were carried out outside clean rooms. Moreover, the pump designs are easily integrated into complex microfluidic systems.

We are further improving the pump design to make it self-priming as well as to use thermal actuation force. Self-priming can be achieved by using thinner PMMA plates, which reduces the pump dead volume. A thermal actuator is being experimented with, and shows promising results. More work is needed for understanding the nonlinearity of the flow rate versus back pressure curve.

Acknowledgments

This work was supported by the academic research fund of the Ministry of Education Singapore, contract number RG11/02. The first author wishes to gratefully acknowledge the PhD scholarship from Nanyang Technological University.

References

[1] Nguyen N T, Truong T Q, Wong K K, Ho S S and Low L N 2004 Micro check valves for integration into polymeric microfluidic devices *J. Micromech. Microeng.* **14** 69–75
[2] van Lintel H T G, van de Pol F C M and Bouwstra S 1998 A piezoelectric micropump based on micromachining of silicon *Sensors Actuators* A **15** 153–67
[3] Esashi M, Shoji S and Nakano A 1989 Normally close microvalve and micropump fabricated on a silicon wafer *Proc. MEMS (Utah, USA)* pp 29–34
[4] Zengerle R, Ulrich J, Kluge S, Richter M and Richter A 1995 A bidirectional silicon micropump *Sensors Actuators* A **50** 81–6
[5] Acero M, Plaza J, Esteve J, Carmono J, Marco S and Samitier J 1997 Design of a modular micropump based on anodic bonding *J. Micromech. Microeng.* **7** 179–82
[6] Nguyen N T, Schubert S, Richer S and Dötzel W 1998 Hybrid-assembled micro dosing system using silicon-based micropump/valve and mass flow sensor *Sensors Actuators* A **69** 85–91
[7] Schabmüller C G J, Koch M, Mokhtari M E, Evans A G R, Brunnschweiler A and Sehr H 2002 Self-aligning gas/liquid micropump *J. Micromech. Microeng.* **12** 420–4
[8] Namasivayam V, Larson R G, Burke D T and Burns M A 2003 Transpiration-based micropump for delivering continuous ultra-low flow rates *J. Micromech. Microeng.* **13** 261–71
[9] Nguyen N T and Wereley S T 2002 *Fundamentals and Applications of Microfluidics* (Boston, MA: Artech House Publishers)
[10] Kämper K P, Döpper J, Ehrfeld W and Oberbeck S 1998 A self-filling low-cost membrane micropump *Proc. MEMS (Heidelberg, Germany)* pp 432–7
[11] Olsson A, Larsson O, Holm J, Lundbladh L, Ohman O and Stemme G 1998 Valve-less diffuser micropumps fabricated using thermoplastic replication *Sensors Actuators* A **64** 63–8
[12] Böhm S, Olthuis W and Bergveld P 1999 A plastic micropump constructed with conventional techniques and materials *Sensors Actuators* A **77** 223–8
[13] Nguyen N T and Truong T Q 2004 A fully polymeric micropump with piezoelectric actuator *Sensors Actuators* B **97** 137–43
[14] Nguyen N T, Huang X Y and Toh K C 2002 MEMS-micropumps: a review *Trans. ASME I* **124** 384–92
[15] Nguyen N T and Huang X Y 2001 Miniature valveless pumps based on printed circuit board technique *Sensors Actuators* A **88** 104–11
[16] Dario P, Croce N, Carrozza M C and Varallo G 1996 A fluid handling system for a chemical microanalyzer *J. Micromech. Microeng.* **6** 95–8